Oxidation behavior of the TiNi shape memory alloy with a laser surface melted layer

C. H. XU
Department of Electronic and Information Engineering, The Hong Kong Polytechnic University, Hunghom, Kowloon, Hong Kong, People's Republic of China

S. Q. SHI*
Department of Mechanical Engineering, The Hong Kong Polytechnic University, Hunghom, Kowloon, Hong Kong, People's Republic of China
E-mail: mmsqshi@polyu.edu.hk

H. C. MAN
Department of Industrial and Systems Engineering, The Hong Kong Polytechnic University, Hunghom, Kowloon, Hong Kong, People's Republic of China

C. H. WOO, C. SURYA
Department of Electronic and Information Engineering, The Hong Kong Polytechnic University, Hunghom, Kowloon, Hong Kong, People's Republic of China

Published online: 4 February 2006

The isothermal oxidation behavior of TiNi specimens with or without laser surface melted (LSM) layers in pure oxygen over the temperature range of 600—800°C was studied. Characterization of the specimens after oxidation was conducted using X-ray diffraction (XRD), scanning electron microscopy (SEM) and energy dispersive spectroscopy (EDS). The oxidation resistance of the LSM specimens has been improved significantly. The formation of a compact oxide layer on the LSM specimens contributes to good oxidation resistance.

1. Introduction

TiNi shape memory alloys (SMAs) have been used in industrial applications as well as many biomedical applications [1, 2] because of its unique properties such as thermal shape memory, particular toxicity, good biocompatibility and corrosion resistance. It is necessary to understand to oxidation properties of the TiNi SMAs as the properties of oxide layers formed during oxidation may play an important role against corrosion. A study on the oxidation of a TiNi alloy at 23°C and 400°C in an oxygen pressure of 10^{-4} Torr or in air revealed the formation of different oxides under different oxidation environments [3]. The oxidation of a TiNi alloy in air and pure oxygen from 300–1000°C has also been reported [4–6].

Surface treatment techniques such as electro-polishing, heat treatment, nitric acid passivation, laser modification have been used to increase the corrosion resistance of TiNi SMAs [7, 8]. The oxidation behavior of a laser surface melted (LSM) layer on a TiNi SMA in pure oxygen gas at a temperature range of 600–800°C is investigated in this paper.

2. Experimental procedure

The material used in the experiment is a commercial hot rolled TiNi plate with a nominal composition of 50.8 Ti and 49.2 Ni. Specimens were cut from the plate, to a size of $10\times2\times2$ mm^3, then ground on emery papers up to 1200 grit, washed in acetone. Some of the polished specimens were treated by a Nd-YAG laser under Ar shielding with the power of 400 W, scanning speed of 40 ms^{-1}, 50% overlapping and beam diameter of 3 mm. The surface of the LSM specimen is smooth (see Fig. 1a). According to EDS composition analysis on the specimen surface, the Ti:Ni ratio of 49:51 for the LSM specimens is close to that for original specimens. The thickness of LSM layer is about 200 μm. The grain size of LSM layer in Fig. 1b is much smaller than that of original specimens in Fig. 1c. The specimen labels in the test are

*Author to whom all correspondence should be addressed.
0022-2461
DOI: 10.1007/s10853-005-3649-1

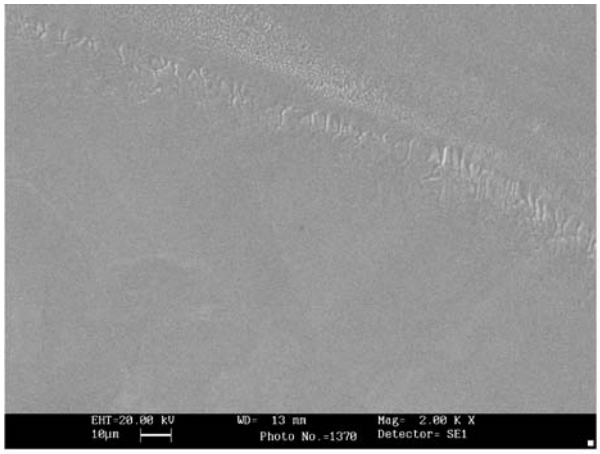

(a)

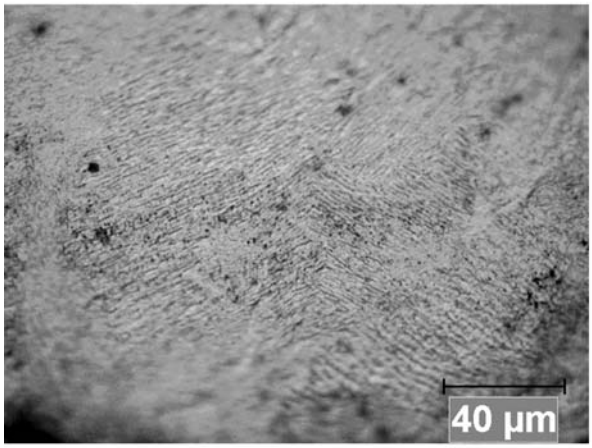

(b)

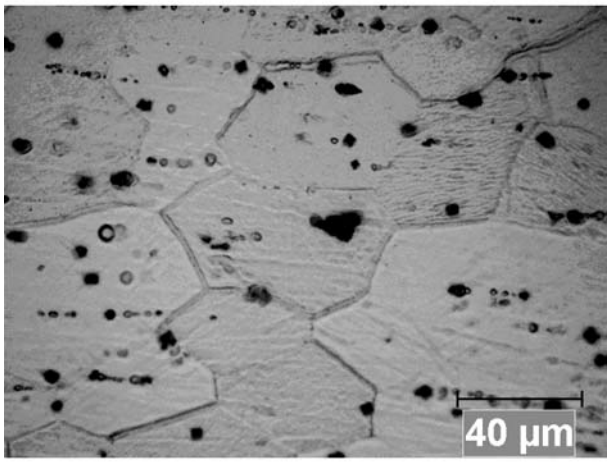

(c)

Figure 1 Microstructure of TiNi alloy showing (a) surface of LSM layer, (b) grains on LSM layer, and (c) grains on original TiNi alloy.

expressed as S — treatment condition (*No* treatment or *Ar* shielding)—oxidation temperature.

Oxidation experiments were performed in a SETARAM LABSYS™ Thermo-gravimetric Analyzer. First, the specimen was heated in protective Ar gas to the oxidation temperature at a heating rate of 50°C/min. Isothermal oxidation was conducted at the temperature range of 600–800°C in 1 atm of oxygen for 20 h. The weight gain of a specimen was measured as a function of time by an electronic balance with an accuracy of 0.1 mg in the thermo-gravimetric analyzer. Finally, the oxidized specimen was cooled to room temperature.

After oxidation, the specimens were examined directly using a Philips PW3710 X-ray Diffraction machine to identify the crystal structures. Cu K_α X-ray was used at 40 kV, 30 mA, and scanning range of 20–70°. The characterization of the oxidized specimens were conducted using a scanning electron microscope (STEREOSCAN 440) equipped with an energy dispersive spectroscope.

3. Results

3.1. Isothermal oxidation kinetics

The oxidation kinetics curves of TiNi alloys with or without a LSM layer are plotted in Fig. 2a–c, showing the weight gains versus time at 600, 700 and 800°C, respectively. The specimens with a LSM layer show better oxidation resistance than the original specimens. The parabolic rate constant (k_p) is determined by the weight gain per unit surface area of a specimen ($\Delta W/A$) and exposure time (t),

$$\left(\frac{\Delta W}{A}\right)^2 = k_p t \tag{1}$$

k_p can be obtained from the slope of a linear regression line on $(\Delta W/A)^2$ vs t plot. The parabolic rate constants obtained from the linear regressions for the different specimens are listed in Table I. High correlation coefficients (R = 0.976–0.99) indicate that the oxidation of TiNi alloys at 600–800° for 20 h obeys the parabolic law.

3.2. Identification of phases on the surface of the oxidized specimens

After isothermal oxidation, the crystal structures on the specimen surfaces were examined by X-ray diffraction

TABLE I Oxidation rate constants k_p ($mg^2\ mm^{-4}\ s^{-1}$) of TiNi alloys at 600–800°C

	Temperature (°C)		
Specimens	600	700	800
S-No-	8.3×10^{-9}	3.1×10^{-8}	1.0×10^{-6}
S-Ar-	2.78×10^{-9}	2.22×10^{-8}	6.1×10^{-7}

TABLE II The identified phases on the surface of oxidized specimens

	Oxidation temperature (°C)		
Specimens	600	700	800
S-No-	TiO_2	TiO_2	TiO_2, $NiTiO_3$
S-Ar-	TiO_2, Ni_3Ti	TiO_2	TiO_2, $NiTiO_3$

and results are listed in Table II. XRD spectra of two types of the specimens after oxidation at 600°C (Fig. 3) show strong (200) TiO_2 peak on S-No-600 specimen, suggesting the rutile TiO_2 oxide with (200) texture. A Ni_3Ti phase was also detected in the S-Ar-600 specimen. The XRD spectra for both types of specimens oxidized at 700 and 800°C are similar, suggesting that oxide products on the outer scales of both types of specimens are the same. A small amount of the $NiTiO_3$ oxide also exists on all specimens after the oxidation at 800°C.

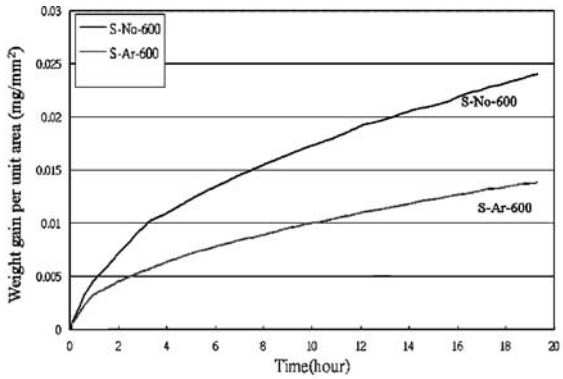

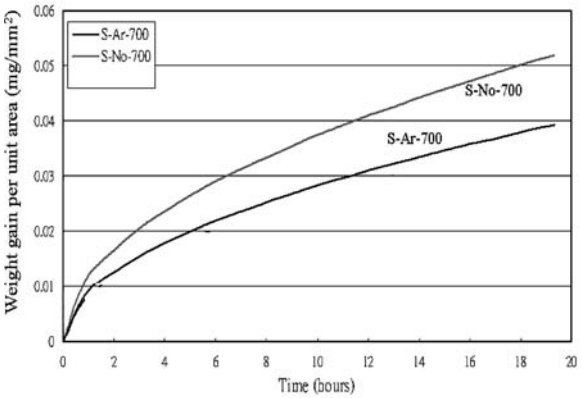

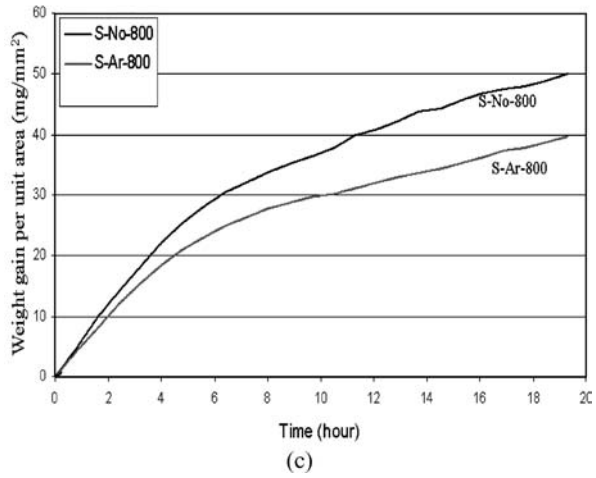

Figure 2 Weight gain versus oxidation time for the isothermal oxidation of TiNi alloys at (a) 600°C, (b) 700°C and (c) 800°C.

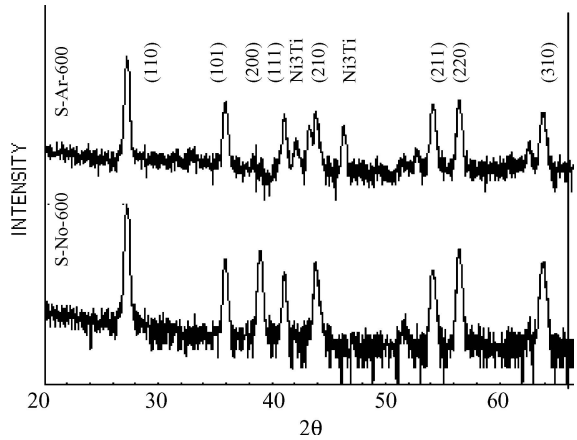

Figure 3 XRD spectra for the specimens with or without LSM layer oxidized at 600°C for 20 h, showing TiO_2 oxide scale on S-No-600 specimen with strong (200) texture and Ni_3Ti phase on S-Ar-600 specimen. (all numbers in the figure are plan indices for TiO_2 oxide).

3.3. Morphologies and micro-composition of oxide scales

The SEM and EDX are used to observe oxide scale and determinate the elemental composition of the oxide layer, respectively. The morphology of the oxide scale formed on the surface of a specimen varied considerably with oxidation temperature.

3.3.1. Oxidation at 600°C

After oxidation at 600°C, the particle size of the oxide on the surface of the specimens in Fig. 4 is small. The surface of the S-No-600 specimen in Fig. 4a is rougher than that of the S-Ar-600 specimen in Fig. 4b. The EDS composition analysis shows Ti oxide formed on the specimen surface. Although a Ni_3Ti phase was detected on the S-Ar-600 specimen by XRD in Table II, no Ni_3Ti layer could not find on the cross section of S-Ar-600 specimen after the oxidation at 600°C. One possible reason is the amount of Ni_3Ti too little to form a layer.

3.3.2. Oxidation at 700°C

The morphologies of the oxide scales formed at 700°C are shown in Fig. 5. The size of oxide particles obtained at 700°C oxidation is much larger than that at 600°C. The oxide particles on the S-No-700 specimen in Fig. 5a are less uniform than those on the S-Ar-700 specimen in Fig. 5b. The EDX result indicates compositions of oxide scale still being mainly titanium and oxygen.

3.3.3. Oxidation at 800°C

The surface morphology of all specimens oxidized at 800°C is similar. The dark area on left-bottom in Fig. 6a is partially spalled oxide scale on the edges of the S-No-800 specimen. As shown in Fig. 6b, the un-spalled scale (white area in Fig. 6a) is similar to the oxide in Figs. 4 and

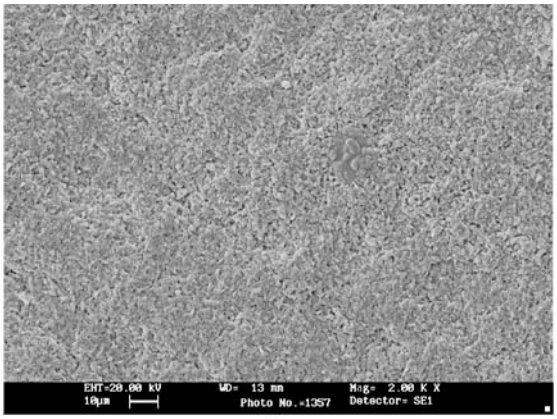

(a)

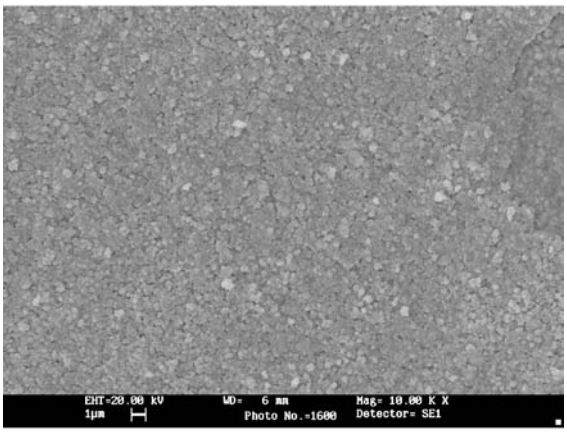

(b)

Figure 4 Scale morphology on TiNi alloy after oxidation at 600°C for 20 h (a) S-No-600, (b) S-Ar-600, showing small oxide particle size and rougher surface on S-No-600.

5, except that the particle size is much more non-uniform. Fig. 6c shows some small holes on the spalled area (dark area in Fig. 6a).

The cross sections of the S-No-800 and S-Ar-800 specimens after oxidation at 800°C are shown in Fig. 6d, e, respectively. Local compositions are detected at the numbered positions (the marks '□' as area or the marks '+' as a point) and EDS analysis on the related positions are listed in Table III. The compact TiO_2 outer layer, loose TiO_2 layer, $TiNi_3$ layer and TiNi substrate can be identified. A small amount of Ni can be detected on the outside oxide layer (position 1) and the inner oxide layer (position 3). The thickness ratio of compact and loose oxides on the S-No-800 and S-Ar-800 specimens is quite different and about 1:5 and 1:1, respectively. The compact and loose TiO_2 layers, but no $TiNi_3$ layer, can also been seen on the cross section of the specimens after oxidation at lower temperatures.

4. Discussions

4.1. The structure of oxide scale

Rutile TiO_2 is the main oxidation product on outer surface for all specimens and some $TiNiO_3$ oxide can be identified

TABLE III Micro-Compositions at the positions in Fig. 6d, e

Specimens	Composition (% at)	Positions 1	2	3	4	5
S-No-800	O	65.5	57.46	67.58	14.65	21.03
in Fig. 6d	Ti	28.7	41.69	30.67	23.00	37.47
	Ni	5.73	0.84	1.75	62.35	41.51
S-Ar-800	O	59.11	60.52	60.89	16.6	21.32
in Fig. 6e	Ti	39.82	3902	36.79	21.88	36.95
	Ni	1.06	0.46	2.32	61.52	41.73

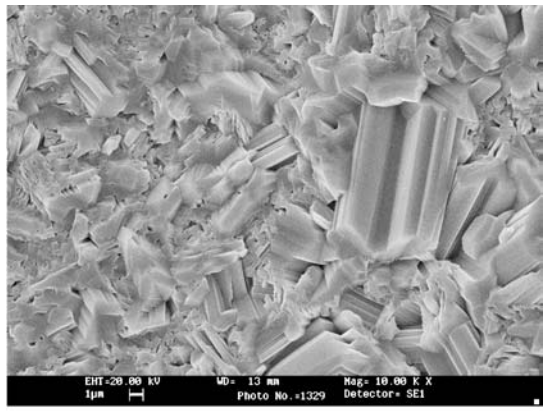

(a)

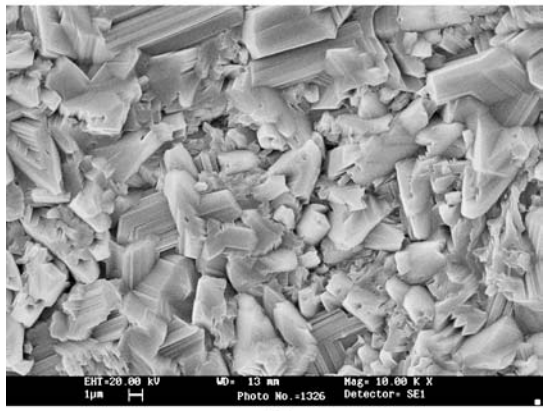

(b)

Figure 5 Scale morphology of TiNi after oxidized at 700°C, showing that oxide particles obtained (a) on the S-No-700 specimen are less uniform than those (b) on the S-Ar-700 specimen.

on the specimens after the oxidation at 800°C by X-ray diffraction (see Table II). As shown in Fig. 6d, e, a complex scale structure, compact TiO_2, loose TiO_2, $TiNi_3$ and TiNi substrate, was formed during high temperature oxidation and small amount of Ni was detected on the outer and inner oxide scales (positions 1 and 3 in Fig. 6d, e. The phases of TiO_2, Ni, $TiNiO_3$ and Ni_3Ti are also detected on the TiNi specimen after oxidation at 800°C in air for 0.5 h by other researchers [4].

The free energy of formation (ΔG) of NiO, TiO_2, $TiNiO_3$, and Ni_3Ti versus temperature is shown in Fig. 7 [9]. Thermodynamically, both Ti and Ni oxides can be formed. Based on the oxidation theory of alloys [10],

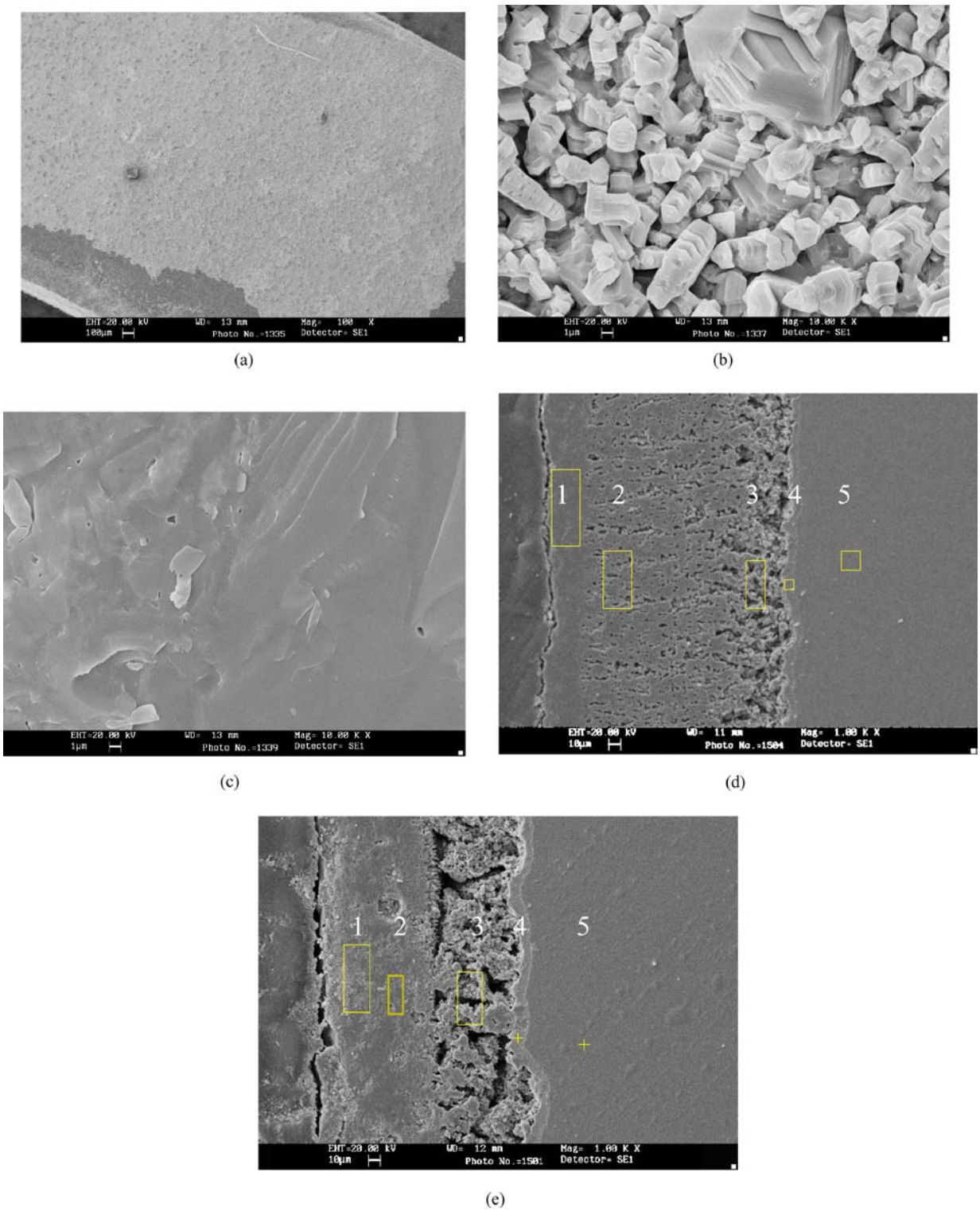

Figure 6 Scale morphology of TiNi after oxidized at 800°C, showing (a) scale spallation (dark area) on the edge of S-No-800 specimen, (b) oxide scale on the un-spalled white area in Fig. 6a, (c) oxide scale on the spalled dark area in Fig. 6a, and the cross sections with the multi-layer structure for (d) the S-No-800 specimen and (e) the S-Ar-800 specimen.

when a clean alloy surface is exposed to an oxidizing atmosphere, NiO and TiO_2 oxides will form on the surface of a specimen. At the same time, the internal oxidation of Ti will occur due to more negative free energy of formation (ΔG) of TiO_2. In other words, TiO_2 can form at lower oxygen pressure (surb-surface). NiO and TiO_2 oxides at the specimen surface will transfer to $TiNiO_3$ to reduce the free energy of formation ΔG further (see Fig. 7). This process continues until a continuous TiO_2 layer form, which is called selective oxidation. Ni at the position 1 in Fig. 6d, e comes from $TiNiO_3$ oxide. $TiNiO_3$ oxide is only detected on the alloy oxidized at 800°C by X-ray diffraction in

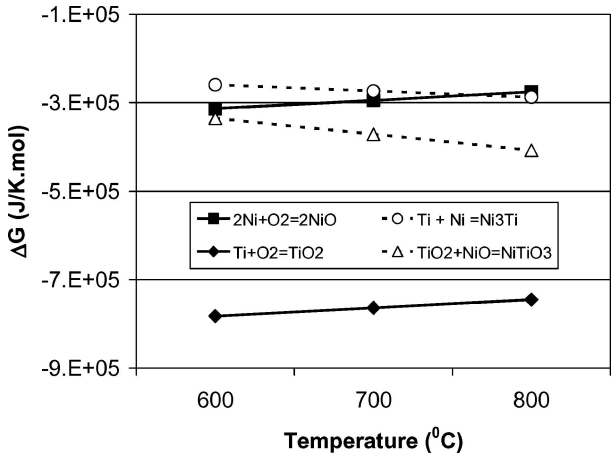

Figure 7 The free energy of formation ΔG of NiO, TiO_2, $TiNiO_3$, Ni_3Ti versus temperature.

Table II. Thermodynamically, the increase in temperature is helpful to form $TiNiO_3$ oxide (see Fig. 7), implying that more $TiNiO_3$ oxide can form at higher temperature before selective oxidation is finished. The amount of $TiNiO_3$ oxide formed at 600 and 700°C may be too little to be detected by X-ray Diffraction. TiO_2 rutile crystals can grow in the vertical and horizontal directions. The voids are possibly formed due to difference between the vertical and lateral growth rates, which results in the formation of a loose oxide structure. As the oxidation progresses, Ti atoms diffuse outward while O atoms diffuse inward. The diffusivity of Ti in rutile is faster than that of oxygen [11], which causes more voids. Less Ti concentration was found beneath the oxide scale due to the formation of Ti oxide. Ni and $TiNi_3$ phases developed there due to depletion of Ti. From the alloy phase diagram, Ti can form a solid solution in Ni (over 10%at Ti in solid solution at 800°C) as Ni(Ti) phase and Ni_3Ti is a stable phase below 1380°C [12]. When oxygen diffused into Ni(Ti) phase, the less noble component Ti (more negative ΔG) was oxidized to form TiO_2 particles caused by low oxygen pressure there, resulting a loose mixture layer of Ni(Ti) and TiO_2. Ni at the position 3 in Fig. 6d, e comes from Ni(Ti). Thermodynamic calculation also indicates TiO_2, $TiNiO_3$ on the scale surface and Ni_3Ti near substrate during TiNi oxidation [4].

4.2. The effects of LSM on oxidation

Comparing with original TiNi specimens, the LSM specimens show a lower oxidation rate in Fig. 2, thicker compact oxide layer in Fig. 6e and less (200) texture of TiO_2 oxide in Fig. 3. The less Ni on the surface of S-Ar-800 (see the position 1 in Table III) indicates that $TiNiO_3$ oxide on the S-Ar-800 surface is less than that on the S-No-800 surface.

Improving oxidation resistance on LSM specimens depends on forming a compact TiO_2 layer. According to Wagner's theory [13], the minimum Ti concentration, N_{Ti} in the alloy to form an external TiO_2 oxide scale can be estimated by

$$N_{Ti} = \left(\frac{\pi g N_O D_O V_m}{3 D_{Ti} V_{OX}} \right)^{\frac{1}{2}} \quad (1)$$

where g is a constant; $N_O D_O$ is the oxygen permeability in the alloy; V_m is molar volume of alloy; D_{Ti} is the diffusion coefficient of Ti; and V_{OX} is the molar volume of the oxide. Ti concentration in TiNi alloy is higher enough to form selective TiO_2 scale. As motioned in 4.1, Ti internally oxidized at the initial oxidation. The penetration velocity of the internal oxidation zone decrease with increasing D_{Ti}, according to Equation 1. The size of grains significantly reduced by a laser surface melted in Fig. 1. The high heating and cooling rates in laser processing cause a state of nonequilibrium of the alloy, such as more crystal defects [14, 15]. Those defects will increase D_{Ti} during oxidation to promote selective oxidation. For this reason, $TiNiO_3$ oxide on the S-Ar-800 surface is less than that on the S-No-800 surface. The decrease in grain size of Ni-20Cr-χAl ($\chi = 2$, 3, 5) [16] and the exposure of cold worked alloys [10] to promote selective oxidation have been reported. On the other hand, the accumulation and lateral growth of the internal oxides is helpful to form a continuous oxide layer [10]. Comparing with original TiNi specimens, Ti atoms in LSM layer diffuse easily along vertical and lateral direction, due to more crystal defects, which can promote the lateral growth of oxide in Fig. 6e and reduce the growth of (200) texture TiO_2 (see Fig. 3). Therefore, the alloy with LSM layer shows lower oxidation rate in Fig. 2.

XRD results in Table II show Ni_3Ti phase in the oxide scale of the S-Ar-600 specimen, but not in other specimens. The thickness of oxide layer on S-Ar-600 is thinner from the analysis on the oxidation kinetic curve in Fig. 2a. Therefore, it is likely that X-ray beam can penetrate oxide scale.

5. Conclusion

Oxidation kinetics for TiNi alloys with or without a LSM layer at 600–800°C for 20 h obeys parabolic law. LSM treatment significantly improves the oxidation resistance of TiNi alloy. The main oxidation product formed on the outer surface of TiNi alloy with or without LSM layers is rutile TiO_2. A multi-layer structure: compact mixture of $TiO_2 \sim TiNiO_3$ oxide layer, loose mixture of Ni(Ti)$\sim TiO_2$ and $TiNi_3$ layer, was formed on the surface of TiNi specimens. LSM treatment for TiNi alloy can reduce the grain size and increase the crystal defects, which helps the lateral diffusion of Ti atoms in the alloy and promotes selective oxidation of Ti to improve the oxidation resistance of the alloy.

Acknowledgements

This work is funded by the Hong Kong Polytechnic University through a grant GYW86 and The Hong Kong Research Grant Council through grants B-Q747

References

1. B. THIERRY, M. TABRIZIAN, C. TREPANIER, O. SAVADOGO and L. H. YAHIA, *J. Biomed. Mater. Res.* **51** (2000) 685.
2. D. J. WEVER, A. G. VELDHUIZEN, J. DE VRIES, H. J. BUSSCHER, D. R. A. UGES and J. R. VAN HORN, *Biomaterials* **19** (1998) 761.
3. C. M. CHAN, S. TRIGWELL and T. DUERING, *Surface and Interface Analysis* **15** (1990) 349.
4. G. S. FIRSTOV, R. G. VITCHEV, H. KUMAR, B. BLANPAIN, J. VAN HUMBEECK, *Biomaterials* **23** (2002) 4862.
5. C. L. CHU, S. K. WU and Y. C. YEN, *Materilas Science and Engineering A* **216** (1996) 193–200.
6. C. H. XU, X. Q. MA, S. Q. SHI and C. H. WOO, *ibid.* **371** (2004) 45.
7. C. TREPANIER, M. TABRIZIAN, L. H. BILODEAU and D. L. PIRON, *J. Biomed. Mater. Res.* **43** (1998) 433.
8. H. C. MAN, Z. D. CUI and T. M. YUE, *Scripta Materialia* **45** (2001) 1447.
9. H. G. LEE, in "Chemical Thermodynamics for Metals and Materials" (Imperial College Press, 1999) p. 275.
10. N. BIRKS and G. H. MEIER, in "Introduction to High Temperature Oxidation of Metals" (Edward Arnold, London, 1983) p. 105.
11. S. A. KEKARE, D. K. SHELTON and P. B. ASWATH, in "Oxidation of High Temperature Intermetallics" (The Minerals, Metals & Materials Society, Warrendale, PA, 1993) p. 325.
12. B. Thaddeus, in "Binary Alloy Phase Diagrams" (ASM International, 1990) p. 2875.
13. C. Z. WAGNER, *Elektrochem.* **63** (1959) 772.
14. G. P. RODRIGUEZ, I. GARCIA, J. DAMBORENEA, *Oxidation of Metals* **58** (2002) 235.
15. L. R. KATIPELLI AND N. B. DAHOTRE, *Materials Science and Technology* **17** (2001) 1061.
16. Z. LIU, W. GAO, K. L. DAHM and F. WANG, *Acta Mater.* **46** (1998) 1691.

Received 19 May 2004
and accepted 25 May 2005